

Article

Mixed Metal Oxides of M1 MoVNbTeO_x and TiO₂ as Composite Catalyst for Oxidative Dehydrogenation of Ethane

Yuxin Chen ^{1,†} , Dan Dang ^{2,†}, Binhang Yan ¹  and Yi Cheng ^{1,*}

¹ Department of Chemical Engineering, Tsinghua University, Beijing 100084, China; chen-yx19@mails.tsinghua.edu.cn (Y.C.); binhangyan@tsinghua.edu.cn (B.Y.)

² School of Chemistry and Chemical Engineering, Henan University of Technology, Zhengzhou 450001, China; dangdan0607@163.com

* Correspondence: yicheng@tsinghua.edu.cn

† Yuxin Chen and Dan Dang contributed equally.

Abstract: Composite catalysts of mixed metal oxides were prepared by mixing a phase-pure M1 MoVNbTeO_x with anatase-phase TiO₂. Two methods were used to prepare the composite catalysts (the simple physically mixed or sol-gel method) for the improvement of the catalytic performance in the oxidative dehydrogenation of ethane (ODHE) process. The results showed that TiO₂ particles with a smaller particle size were well dispersed on the M1 surface for the sol-gel method, which presented an excellent activity for ODHE. At the same operating condition (i.e., the contact time of 7.55 g_{cat}·h/molC₂H₆ and the reaction temperature of 400 °C), the M1-TiO₂-SM and M1-TiO₂-PM achieved the space time yields of 0.67 and 0.52 kgC₂H₄/kg_{cat}/h, respectively, which were about ~76% and ~35% more than that of M1 catalyst (0.38 kgC₂H₄/kg_{cat}/h), respectively. The BET, ICP, XRD, TEM, SEM, H₂-TPR, C₂H₆-TPSR, and XPS techniques were applied to characterize the catalysts. It was noted that the introduction of TiO₂ raised the V⁵⁺ abundance on the catalyst surface as well as the reactivity of active oxygen species, which made contribution to the promotion of the catalytic performance. The surface morphology and crystal structure of used catalysts of either M1-TiO₂-SM or M1-TiO₂-PM remained stable as each fresh catalyst after 24 h time-on-stream tests.

Keywords: ODHE; ethylene; mixed metal oxides; MoVNbTeO_x; TiO₂



Citation: Chen, Y.; Dang, D.; Yan, B.; Cheng, Y. Mixed Metal Oxides of M1 MoVNbTeO_x and TiO₂ as Composite Catalyst for Oxidative Dehydrogenation of Ethane. *Catalysts* **2022**, *12*, 71. <https://doi.org/10.3390/catal12010071>

Academic Editors: Hugo de Lasa and Mohammad Mozahar Hossain

Received: 22 December 2021

Accepted: 7 January 2022

Published: 9 January 2022

Publisher's Note: MDPI stays neutral with regard to jurisdictional claims in published maps and institutional affiliations.



Copyright: © 2022 by the authors. Licensee MDPI, Basel, Switzerland. This article is an open access article distributed under the terms and conditions of the Creative Commons Attribution (CC BY) license (<https://creativecommons.org/licenses/by/4.0/>).

1. Introduction

Ethylene is a principal chemical commodity and an essential petrochemical building block, for example, to produce polyethylene, the most extensively used plastic in the chemical industry [1–3]. The oxidative dehydrogenation of ethane (ODHE) to ethylene has been recognized as the most attractive alternative to the conventional steam cracking process due to its low energy demand, mild exothermic properties, high productivity of ethylene, and little risk of carbon deposition [4,5]. Among the numerous catalysts studied in the ODHE process [5–24], the MoVNbTeO_x catalyst possesses the merit of higher catalytic performance (e.g., ethylene selectivity and productivity) at lower temperature [5,9,10,19,24], which is synthesized by the hydrothermal [25] or slurry [26] method and composed of M1, M2, and some minor phases [27]. The M1 (orthorhombic phase) is mainly responsible for the ODHE reaction, while M2 (pseudo-hexagonal phase) shows a poor or even negative effect during the ODHE process [10,28]. The phase-pure M1 catalysts can be obtained from the mixed metal oxides after dissolving the M2 crystalline and other phases in MoVNbTeO_x [29]. The M1 phase is a two-dimensional projection of the polyhedral network in the crystallographic (001) plane, in which the pentagonal Nb-centered pillars are surrounded by edge and corner-sharing MoO₆ and VO₆ octahedra and these pentagonal units are connected with metal oxygen octahedra to form hexagonal and heptagonal channels, which are partially occupied by Te. Moreover, the V⁵⁺ ions at the active sites are responsible for the abstraction

of the first C–H bond in ethane [5,30,31]. The M2 phase has characteristic hexagonal rings hosting the Te–O units without any pentagonal or heptagonal rings in the (001) plane [32].

The purification process can be implemented by the hydrothermal method with a strict preparation procedure or by post-treatment [10,33,34]. In order to meet the demand for the commercialization of the ODHE process, e.g., a 60% ethylene yield and a 1.00 kg_{C₂H₄}/kg_{cat}/h productivity at below 500 °C [19,35–37], the catalytic performance should be enhanced, and a lot of work has been performed in recent years [38–48]. As one of the possible solutions, it would be worth trying to introduce additives or promoters to increase the activation sites (e.g., V⁵⁺ ions on the phase-pure M1) so as to promote the catalytic efficiency. To be noted, several successful attempts have been achieved in the literature. By the combination of CeO₂ or MnO_x with phase-pure M1 catalysts, composite catalysts markedly enhance the catalytic performance for the ODHE process [9,44,45,49], which provides a possibility and preliminary verification on adding cheaper promoters to increase the catalytic activities of MoVNbTeO_x catalysts. TiO₂ as an effective promoter/catalyst has been widely used in catalytic processes [50–52]. Holmberg et al. [53] used TiO₂ as a diluter to study the catalytic performance for propane ammoxidation. They mixed the Mo–V–Nb–Te precursors (slurry method) with TiO₂ sol (the TiO₂ phase is formed) and evaporated the mixture to obtain the MoVNbTeO_x/TiO₂ catalyst. However, Mo_{5–x}(V/Nb/Te)_xO₁₄, instead of the M1 phase, was formed, and the prepared catalysts did not demonstrate an increase in activity. Li et al. [54] studied of the support and promotion effect of TiO₂ for the selective oxidation of ethane to acetic acid catalyzed by Mo–V–Nb oxides. They prepared a Mo_{0.61}V_{0.31}Nb_{0.08}O_x/TiO₂ catalyst by the slurry method, where a MoVNb catalyst was directly loaded on TiO₂ particles. Che-Galicia et al. [55] studied the mass and heat transfer in an industrial packed-bed reactor using TiO₂ as a MoVNbTeO_x catalyst carrier (MoVTeNbO/TiO₂) for the oxidative dehydrogenation of ethane to the ethylene reactor. TiO₂ is only a catalyst carrier to form particles for industrial applications, and the catalyst–carrier interaction between TiO₂ and M1 is not considered. Nevertheless, these researches have not reported the effective enhancement of the catalytic performance of MoVNbTeO_x catalysts.

In our recent work, a sol-gel method was used to prepare M1–TiO₂ nano-composite catalysts, which showed a positive influence on the catalytic performances of M1 catalysts [56]. This work aimed to investigate how the contact pattern between M1 and TiO₂ particles affected the catalytic performance and unveiled the synergistic effect of M1 and TiO₂ in the catalytic process. We adopted two different methods to prepare the M1–TiO₂ nanocomposite oxide catalysts with different contact interactions between M1 and TiO₂. The phase-pure M1 and TiO₂ were mixed at the macro- or micro-scales by the physical mixing or sol-gel methods, respectively. The potential mechanisms were explained by different characterization techniques, which can provide new insights on how to manipulate the catalytic performance of M1-based catalysts for ODHE.

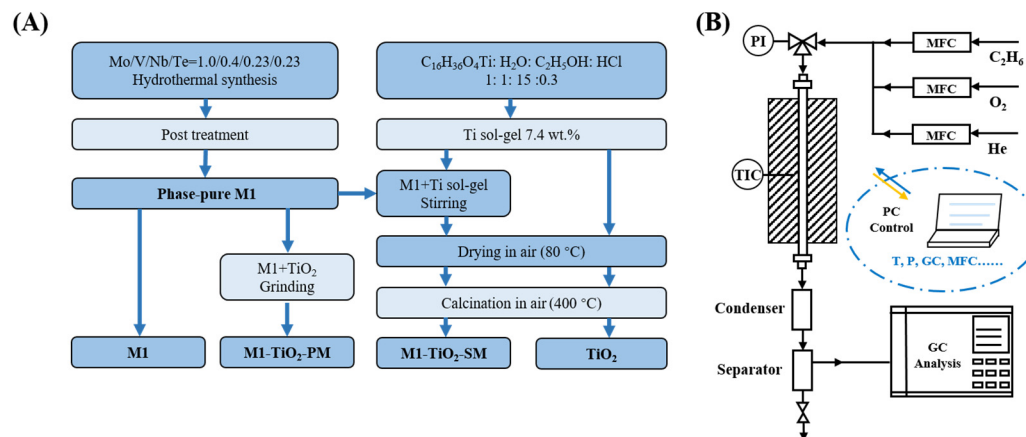
2. Experimental

2.1. Preparation of Catalysts

MoVNbTeO_x mixed metal oxide was synthesized hydrothermally via an aqueous solution composed of ammonium heptamolybdate (99.0%; Sigma-Aldrich, Darmstadt, Germany), vanadyl sulfate (97%; Sigma-Aldrich, Tokyo, Japan) telluric acid (98%; Sigma-Aldrich, Tokyo, Japan), and ammonium niobium oxalate (99.99%; Sigma-Aldrich, Darmstadt, Germany), on the basis of the procedure reported in the literature [9,57]. The aqueous solution contained Mo, V, Te, and Nb at a molar ratio of 1:0.25:0.23:0.18. The lump solid obtained was ground to the powder form mainly consisting of phases M1 and M2. The phase-pure M1 was achieved by the post-treatment to remove the M2 phase using 30% HNO₃.

Titanium sol was prepared as follows: tetrabutyl titanate (Sinopharm Chemical Reagent Co., Ltd., Shanghai, China), deionized water, anhydrous alcohol (Sinopharm Chemical Reagent Co., Ltd.), and hydrochloric acid (Sinopharm Chemical Reagent Co., Ltd.,

Shanghai, China) were mixed thoroughly at a $C_{16}H_{36}O_4Ti:H_2O:C_2H_5OH:HCl$ molar ratio of 1:1:15:0.3, forming a stable transparent sol with 7.4 wt % TiO_2 . Titanium sol was dried overnight at 80 °C and calcined in air for 6 h at 400 °C in a muffle furnace to obtain a TiO_2 sample. The preparation procedure of the catalysts is shown in Scheme 1A.



Scheme 1. (A) Synthesis procedure of different catalysts; and (B) fix-bed system for the catalytic activity test.

As mentioned above, the major concern of this work was to present the influence of the preparation method of M1– TiO_2 composite catalysts on the catalytic performance in ODHE process. Two methods were employed to synthesize the catalysts of M1– TiO_2 , where 40 wt % TiO_2 was chosen as an optimized composition based on our earlier work [56]. Firstly, the simplest way to make the composite catalyst was the physical mixing, i.e., solid TiO_2 was milled together with the phase-pure M1 at a mass ratio of 2:3 and then ground mechanically for 10 min. In this way, the obtained catalyst was named as M1-40 TiO_2 -PM. Secondly, the sol-gel method was employed to have the M1 mixed with TiO_2 more intimately at the micro-scale. That is, the phase-pure M1 was mixed with the titanium sol at a mass ratio of 9:1, stirred in a 60 °C water bath for 2 h and dried overnight at 80 °C. After the activation by calcination in air for 6 h at 400 °C with the heating rate of 5 °C/min in the muffle furnace, the obtained catalyst was named as M1-40 TiO_2 -SM.

2.2. Characterization of Catalysts

The Brunauer-Emmett-Teller specific surface area (BET), inductively coupled plasma optical emission spectrometer (ICP-OES), X-rays diffraction (XRD), transmission Electron Microscope (TEM), scanning electron microscope (SEM), and X-ray photoelectron spectroscopy (XPS) techniques were applied to characterize the catalysts, which is consistent with our previous work [45,58]. A H_2 temperature-programmed reduction (H_2 -TPR) measurement was conducted in a quartz tube (inner diameter 4 mm), and 10 mg sample were used in analysis. Prior to analysis, the catalyst was purged for 30 min at 200 °C in an Ar stream at a flow rate of 20 mL/min and then cooled to 50 °C. Then, the gas flow was switched to a 10% H_2 /Ar flow at a flow rate of 20 mL/min by a 6-way valve and ramped from 50 to 800 °C at 10 °C/min. A thermal conductivity detector (TCD) detector (8860 GC system, Agilent) was used to measure H_2 consumption during the process. A C_2H_6 temperature-programmed surface reaction (C_2H_6 -TPSR) experiment was performed in a quartz tube (4 mm i.d.), and 20 mg sample were used in analysis. Prior to analysis, the catalyst was purged for 30 min at 200 °C in a N_2 stream at a flow rate of 20 mL/min. Then, the gas flow was switched to a 25% C_2H_6 / N_2 flow at a flow rate of 20 mL/min and ramped from 200 to 700 °C at 10 °C/min. The outlet gas was detected by an on-line FTIR (Nicolet-is50; Thermo Fisher). For all used catalysts, the reaction condition was a reaction temperature of 400 °C and a contact time of 18.52 $g_{cat} \cdot h / mol_{C_2H_6}$ at the ambient pressure, the inlet molar ratio of $C_2H_6/O_2/He$ was 30/20/50, and the reaction time was

about 24 h. Laser Raman spectra were recorded at the ambient temperature in air with a 325 nm laser excitation on a HORIBA Raman Spectrometer (LabRAM HR Evolution Raman Spectrometer, HORIBA). The laser power on the sample was 3.2 mW, and the integration time was 60 s 4 times for each spectrum.

2.3. Evaluation of the Catalysts

The prepared catalyst samples were evaluated in a quartz tubular reactor (8 mm i.d.; 600 mm in length) at the atmospheric pressure for the ODHE process. For each series of experiments, 0.3 g catalyst was diluted by 3.0 g SiC particles with a size of about 200 μm to weaken the heat effect on the temperature distribution in the packed bed [41]. The compositions of the reactant gases at the inlet were given as 30% C_2H_6 , 20% O_2 , and 50% He (molar ratio), which referred to the literature as a reasonable base to compare the reaction performances [57]. The contact time was defined as $W/F_{\text{C}_2\text{H}_6}$ (where W is the mass of the catalyst and $F_{\text{C}_2\text{H}_6}$ is the ethane molar flow rate), and the total flow rate was varied from about 22 to 55 mL/min, corresponding to the contact time of 7.55–18.52 $\text{g}_{\text{cat}}\cdot\text{h}/\text{mol}_{\text{C}_2\text{H}_6}$.

Intrinsic kinetic analysis was performed according to the conditions of the reference literature [59]. In order to exclude the effect of the mass and the heat transfer in the fixed bed, about 20–40 mg catalyst were diluted by SiC particles to a total mass of 1100 mg, using a total gas flow of 30 mL/min during the whole process and keeping the $X_{\text{C}_2\text{H}_6}$ smaller than ~5%. The partial pressures of C_2H_6 were 10/20/30 kPa and those of O_2 were 10/15/20 kPa (He as a balance gas) were used to determine the order dependence of the reaction on the reactants. For the activation energy determination, the inlet reactant molar ratio ($\text{C}_2\text{H}_6/\text{O}_2/\text{He}$) of 30/20/50 was used at the temperature range of 360–440 $^\circ\text{C}$.

An on-line Shimadzu GC 2014 equipped with a TCD detector was used to measure the compositions of the reactants and the products, in which two columns were used to separate the products (a PorapakQ column for CO_2 , C_2H_4 , and C_2H_6 and a 5A molecular sieve column for O_2 and CO). The conversion of ethane and the selectivity to products were calculated as follows:

$$X_{\text{C}_2\text{H}_6} = \left(1 - \frac{2f_{\text{C}_2\text{H}_6}}{2f_{\text{C}_2\text{H}_6} + 2f_{\text{C}_2\text{H}_4} + f_{\text{CO}} + f_{\text{CO}_2}}\right) \times 100\%, \quad (1)$$

$$S_{\text{C}_2\text{H}_4} = \frac{2f_{\text{C}_2\text{H}_4}}{2f_{\text{C}_2\text{H}_4} + f_{\text{CO}} + f_{\text{CO}_2}} \times 100\%, \quad (2)$$

$$S_{\text{CO}} = \frac{f_{\text{CO}}}{2f_{\text{C}_2\text{H}_4} + f_{\text{CO}} + f_{\text{CO}_2}} \times 100\%, \quad (3)$$

$$S_{\text{CO}_2} = \frac{f_{\text{CO}_2}}{2f_{\text{C}_2\text{H}_4} + f_{\text{CO}} + f_{\text{CO}_2}} \times 100\%, \quad (4)$$

where $X_{\text{C}_2\text{H}_6}$ is the ethane conversion, S is the selectivity to a certain product, and f is the molar fraction in the effluent gas. The diagram of fix-bed system for the catalytic activity test is shown in Scheme 1B.

3. Results and Discussion

3.1. Reaction Performance in the ODHE Process

3.1.1. Catalytic Performance

Figure 1 shows the catalytic performances of the catalysts at different reaction temperatures and contact times. The main products included ethylene, carbon monoxide, and carbon dioxide, whereas a very small amount of acetic acid was ignored [60]. It can be seen that TiO_2 itself had almost no catalytic activity for the selective oxidative dehydrogenation of ethane to ethylene over a wide range of temperatures and contact times for the ODHE reaction, which showed a ~12% ethane conversion with a ~3% ethylene selectivity at the reaction temperature of 400 $^\circ\text{C}$ and a contact time of 18.52 $\text{g}_{\text{cat}}\cdot\text{h}/\text{mol}_{\text{C}_2\text{H}_6}$. In addition, the performances of the catalysts M1, M1-40 TiO_2 -SM, and M1-40 TiO_2 -PM were typical of

the oxidative transformations of hydrocarbons as reported in the literature [24]. However, the addition of TiO₂ can significantly promote the catalytic performance, no matter which method was employed to add the TiO₂ to the phase-pure M1.

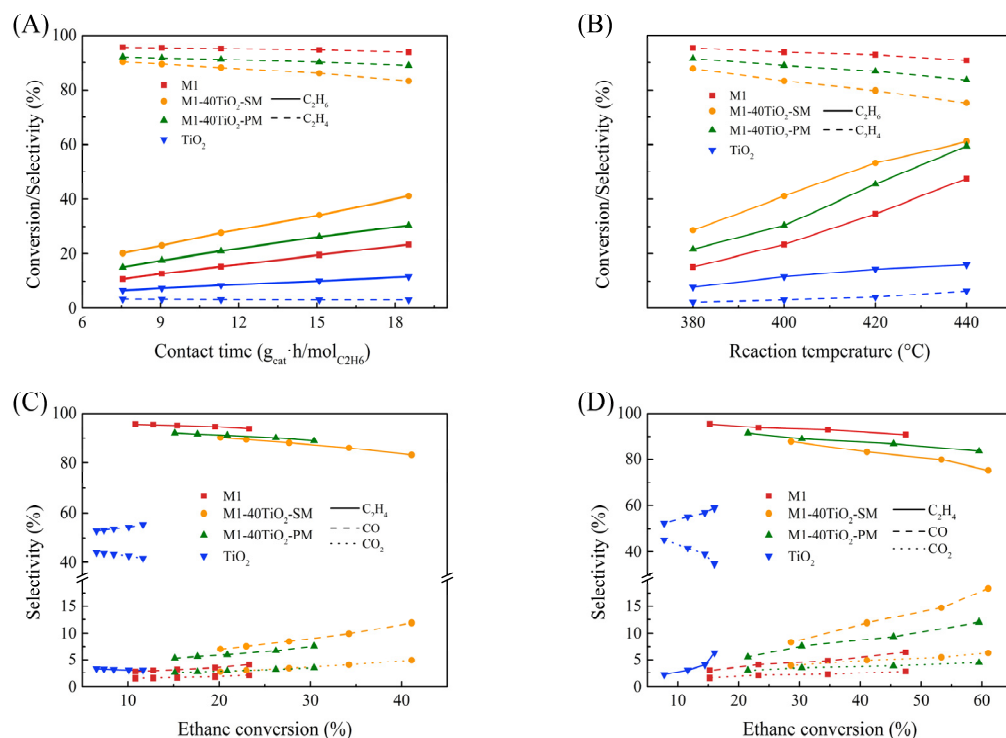


Figure 1. (A) Ethane conversion and products selectivity as a function of the contact time; (B) products selectivity as a function of the ethane conversion in the oxidative dehydrogenation of ethane (ODHE) process at the reaction temperature of 400 °C; (C) ethane conversion and products selectivity as a function of reaction temperature; and (D) products selectivity as a function of the ethane conversion in the ODHE process at the contact time of 18.52 g_{cat}-h/mol_{C₂H₆}. Reaction conditions: ambient pressure and the C₂H₆/O₂/He molar ratio = 30/20/50 at the reactor inlet.

As shown in Figure 1A, the conversion of ethane rose linearly with the increase of the contact time, while the selectivity of ethylene decreased because of the over-oxidation of ethane/ethylene to carbon oxides. Interestingly, in spite of the fact that the M1-40TiO₂-SM catalyst displayed an obvious advantage in the ethane conversion at the same conditions, the M1-40TiO₂-PM catalyst showed a higher ethylene selectivity at the same ethane conversion than the M1-40TiO₂-SM catalyst (Figure 1B). As presented in Figure 1C, increasing the reaction temperature could significantly enhance the catalytic performances of all the samples. Generally, because the Arrhenius rate increases with temperature [61], which can explain the tendency of the ethane conversion rising linearly with the increase of the reaction temperature. As mentioned above, catalysts M1, M1-40TiO₂-SM, and M1-40TiO₂-PM showed similar trends in selectivity for ethylene (Figure 1D). The increase of the ethane conversion and the decrease of the ethylene selectivity resulted from the deep over-oxidation in the ODHE reaction.

Figure 2 shows the space-time yields (STYs) of ethylene at different reaction conditions. At the reaction temperature of 400 °C (Figure 2A), the STY decreased with the increasing contact time, which was related to the fact that the ODHE reaction was the first-order dependence on ethane. Conversely, the temperature had a positive effect on the STY (Figure 2B). At the contact time of 7.55 g_{cat}-h/mol_{C₂H₆} and the reaction temperature of 400 °C, the STY of ethylene of the M1-40TiO₂-SM catalyst was 0.67 kg_{C₂H₄}/kg_{cat}/h, while that of the M1-40TiO₂-PM catalyst was 0.52 kg_{C₂H₄}/kg_{cat}/h, which were 76% and 35% more than that of the phase-pure M1 (0.38 kg_{C₂H₄}/kg_{cat}/h), respectively. In addition, the

M1-40TiO₂-SM catalyst presented a higher catalytic activity than that of the M1-40TiO₂-PM catalyst in a wide range of reaction temperatures and contact times.

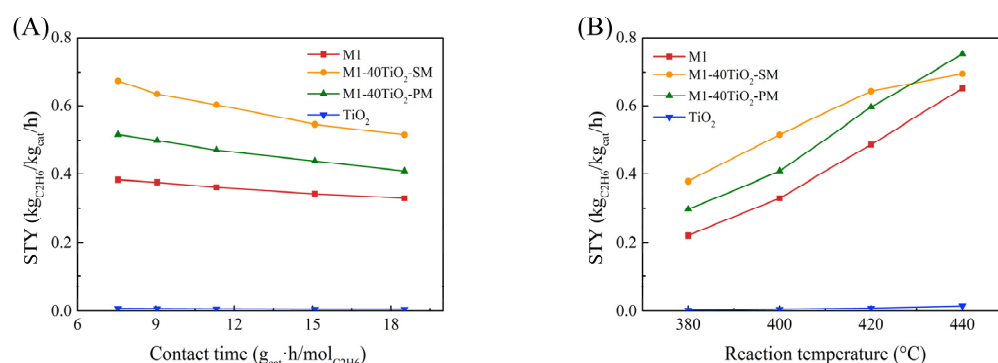


Figure 2. (A) Space time yield of ethylene as a function of the contact time at the reaction temperature of 400 °C; and (B) space-time yield as a function of the reaction temperature at the contact time of 18.52 g_{cat}·h/mol_{C₂H₆} in the ODHE process. Reaction conditions: ambient pressure and the C₂H₆/O₂/He molar ratio = 30/20/50 at the reactor inlet.

As shown in Figure 3 and Table 1, the activation energies for the ethane conversion were 91.4 kJ/mol for M1 and 82.3/88.4 kJ/mol for M1-40TiO₂-SM/PM. At the same time, the order dependence of the response to C₂H₆ and O₂ was only slightly changed, which was similar to the ODHE reaction following the MvK mechanism reported in the literature [46,62]. However, the difference in the activation energy of about 8 kJ/mol and the reaction order were not sufficient to demonstrate a change in the reaction mechanism [19]. Furthermore, the different preparation methods (sol-gel or physical mixing methods) showed a different activation energy and reaction order dependence on C₂H₆, which implied a difference in the interaction between M1 and TiO₂. Meanwhile, both samples with the sol-gel and physical mixing methods showed an increase in the reaction order dependence on O₂, which implied the changes in oxygen species after introducing TiO₂ into the M1 phase.

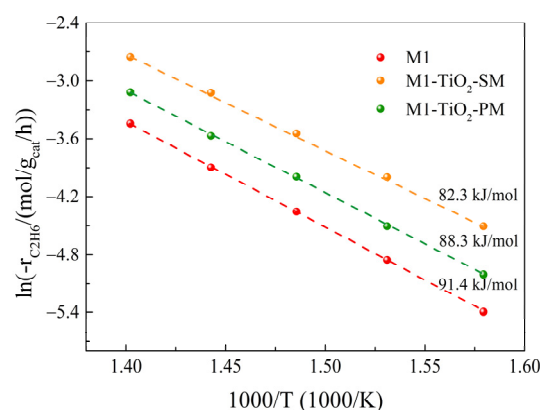


Figure 3. Arrhenius plots for M1, M1-40TiO₂-SM, and M1-40TiO₂-PM.

Table 1. Kinetic parameters for the ODHE process ($-r_{C_2H_6} = A_0 \cdot \exp(-Ea/RT) \cdot P_{C_2H_6}^\alpha \cdot P_{O_2}^\beta$).

Catalyst	α	β	ODHE Ea (kJ/mol)
M1	0.90	0.02	91.4
M1-40TiO ₂ -SM	0.99	0.06	82.3
M1-40TiO ₂ -PM	0.90	0.06	88.4

3.1.2. Catalyst Stability

Time-on-stream experiments in 24 h were performed to investigate the catalytic stability of the samples (Figure 4). As shown in Figure 4, the catalytic performances of the phase-pure M1 catalyst and TiO_2 were stable in 24 h time-on-stream tests. The ethane conversion of the M1-40 TiO_2 -SM catalyst had a certain decrease, and the ethylene selectivity had a corresponding increase with the progress of the reaction time. Interestingly, instead of reduction, both the ethane conversion and ethylene selectivity of the M1-40 TiO_2 -PM catalyst exhibited slightly improvements with the progress of the reaction time in 24 h.

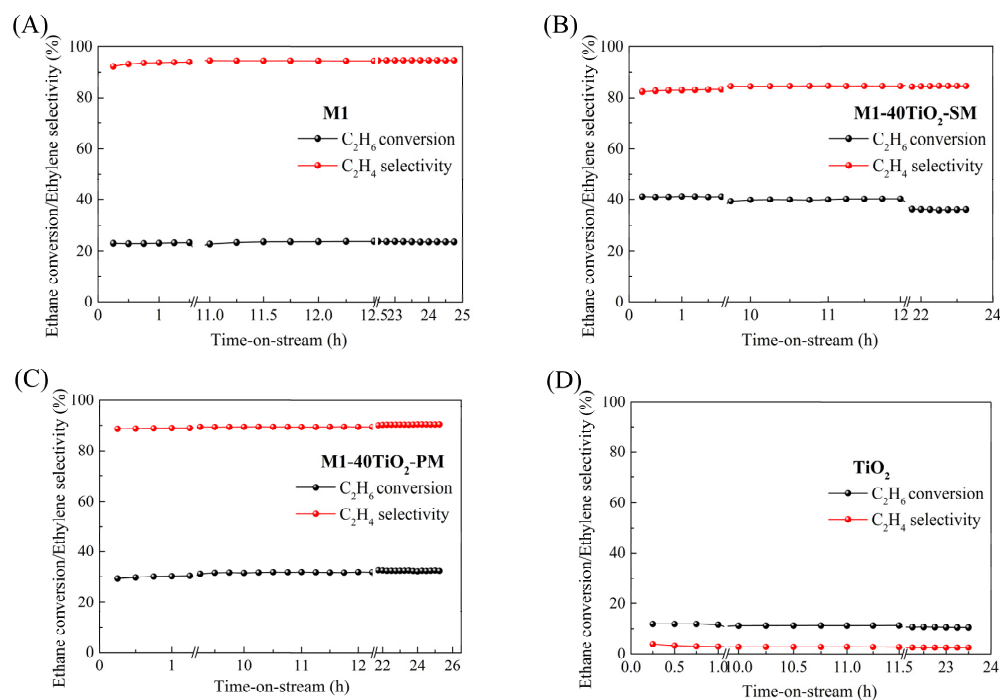


Figure 4. Ethane conversion and ethylene selectivity as a function of the reaction time for the catalysts: (A) M1; (B) M1-40 TiO_2 -SM; (C) M1-40 TiO_2 -PM; and (D) TiO_2 .

3.2. Catalyst Characterization

3.2.1. Elemental Compositions and Textural Properties

The bulk compositions of the samples were measured by ICP-OES, as shown in Table 2. The addition of TiO_2 to the phase-pure M1 by the sol-gel method and the physical mixing method had no effect on the bulk metal content of the phase-pure M1, while it significantly increased the surface areas and changed the pore volumes of the M1-40 TiO_2 -SM and M1-40 TiO_2 -PM catalysts as given in Tables 2 and 3. This increase was much larger than the addition of other elements to the M1 phase [9,24,63]. Compared with fresh catalysts, the used catalysts M1, M1-40 TiO_2 -SM, and M1-40 TiO_2 -PM showed the relative stable characteristics in terms of the specific surface area and the pore volume, which may explain the reason for the stability of the catalytic performances of those catalysts in the 24 h time-on-stream experiments.

Table 2. Compositions of the phase-pure M1 MoVNbTeO_x - TiO_2 catalysts.

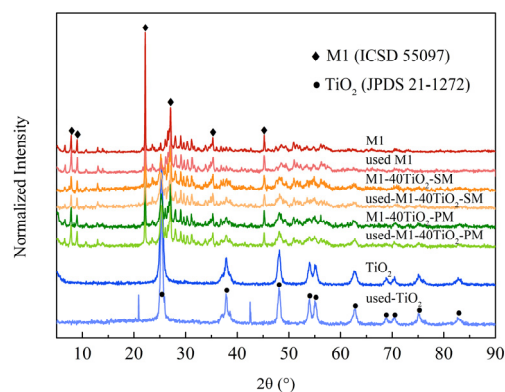
Catalyst	TiO_2 Content (wt %)	Bulk Composition
M1	-	$\text{MoV}_{0.25}\text{Nb}_{0.24}\text{Te}_{0.12}$
M1-40 TiO_2 -SM	39.6	$\text{MoV}_{0.25}\text{Nb}_{0.24}\text{Te}_{0.12}$
M1-40 TiO_2 -PM	40.0	$\text{MoV}_{0.25}\text{Nb}_{0.24}\text{Te}_{0.12}$

Table 3. Textural characterization of the phase-pure M1 MoVNbTeO_x-TiO₂ catalysts.

Catalysts	Specific Surface Area (m ² /g)	Pore Volume (cc/g)
M1	17.7	0.060
Used M1	15.7	0.048
M1-40TiO ₂ -SM	52.4	0.085
Used M1-40TiO ₂ -SM	49.6	0.080
M1-40TiO ₂ -PM	36.3	0.066
Used M1-40TiO ₂ -PM	36.1	0.063
TiO ₂	52.7	0.104

3.2.2. XRD

Figure 5 shows the XRD patterns of the samples. The typical characteristic peaks of the M1 (ICSD 55097; $2\theta = 6.6^\circ, 7.7^\circ, 8.9^\circ, 10.7^\circ, 22.1^\circ, 27.2^\circ, 29.2^\circ,$ and 35.48°) [64] and the anatase-phase TiO₂ (JPDS 21-1272; $2\theta = 25.4^\circ, 37.9^\circ, 48.2^\circ, 53.8^\circ, 54.1^\circ, 62.6^\circ, 70.5^\circ,$ and 75.1°) [65] were observed, and no other crystalline peaks were detected. The full widths at half maximum (FWHMs) of these peaks decreased after introducing TiO₂, which implied an increase in the size of the crystalline domain of the anatase phase. It also can be seen that no significant change was detected in the XRD patterns of the used catalysts comparing with in the XRD patterns of the fresh catalysts, suggesting that the catalytic performances of the samples may be partly attributed to the stable crystal structures of the catalysts.

**Figure 5.** XRD patterns of the fresh and used catalysts (M1, M1-40TiO₂-SM, and M1-40TiO₂-PM).

3.2.3. Catalysts Morphologies

Figure 6A–F presents the surface micrographs of the catalysts M1 catalyst, M1-40TiO₂-SM, and M1-40TiO₂-PM, together with those of the used ones in the ODHE process. Figure 6A shows M1-phase crystals with a rod-like morphology and an average width of ~100 nm and an average length of ~200 nm, which is consistent with those in the literature [9]. The SEM image (Figure 6B) shows well-dispersed TiO₂ particles on the surface of the M1-40TiO₂-SM catalyst. While for the M1-40TiO₂-PM catalyst, the TiO₂ particles were not adhered uniformly to the surface of the phase-pure M1, and the size of rodlike M1 decreased obviously, resulting from being ground mechanically with TiO₂, which may cause a slight improvement of the catalytic activity of the M1-40TiO₂-PM catalyst in the 24 h time-on-stream experiment. The TEM images (Figure 7B,C) showed two different crystals observed in the catalysts M1-40TiO₂-SM and M1-40TiO₂-PM, which represented phase-pure M1 and TiO₂, respectively. Comparing Figure 6B,C and Figure 7B,C, the attachment of TiO₂ added to the phase-pure M1 by the sol-gel method was greater than that by the physical mixing method, which was in agreement with the appearance of the SEM images. No obvious change was observed in the SEM and TEM images of the used catalysts M1, M1-40TiO₂-SM, and M1-40TiO₂-PM, illustrating the structural stability of the catalysts.

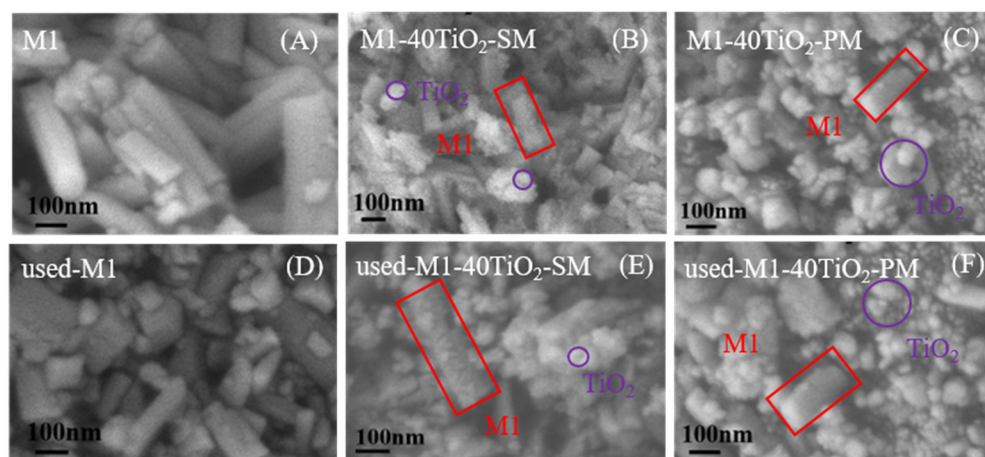


Figure 6. SEM images: (A) fresh M1; (B) fresh M1-40TiO₂-SM; (C) fresh 40TiO₂-PM M1; (D) used M1; (E) used M1-40TiO₂-SM; (F) used M1-40TiO₂-PM.

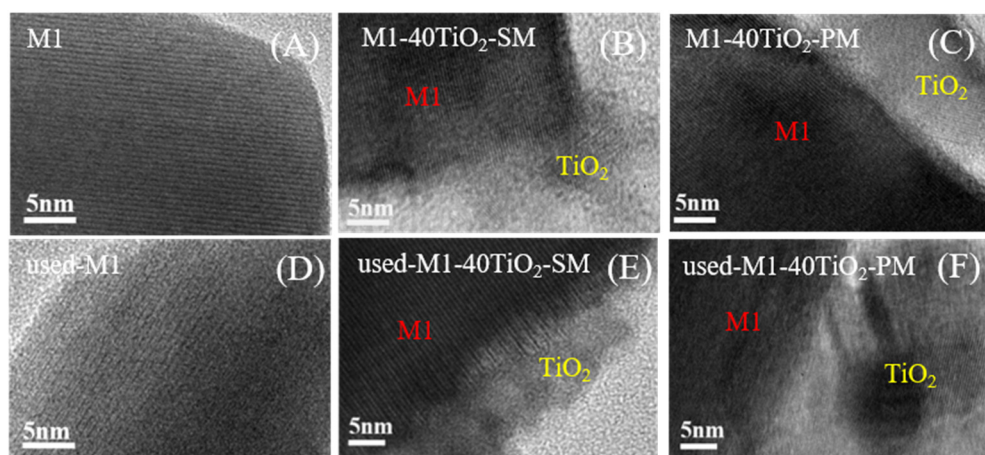


Figure 7. TEM images: (A) fresh M1; (B) fresh M1-40TiO₂-SM; (C) fresh 40TiO₂-PM M1; (D) used M1; (E) used M1-40TiO₂-SM; (F) used M1-40TiO₂-PM.

3.2.4. XPS Analysis

The XPS spectra of the key elements in the fresh and used catalysts M1, M1-40TiO₂-SM, and M1-40TiO₂-PM were analyzed to study the influence of the TiO₂ introduction on the element valence states of the catalyst surface. The binding energy data of the reference material were obtained from the NIST X-ray Photoelectron Spectroscopy Database.

As presented in Figure 8, the binding energy of Mo 3d (232.9 ± 0.2 eV) was similar to the value of 232.8 eV typically reported for MoO₃; the binding energy of Nb 3d (207.2 ± 0.2 eV) was identical to 207.2 eV typically reported for Nb₂O₅; the binding energy of Te 3d (576.3 ± 0.2 eV) was the same as the value of 576.3 eV as reported for TeO₂; and the binding energy of Ti 2p (458.5 ± 0.1 eV) was similar to 458.4 eV reported for TiO₂, corresponding to valence states of Mo⁶⁺, Nb⁵⁺, Te⁴⁺, and Ti⁴⁺, respectively [3,9,60]. Introducing TiO₂ to the phase-pure M1 did not affect the valence states of elements Mo, Nb, Te, and Ti in catalysts M1-40TiO₂-SM and M1-40TiO₂-PM. However, the surface composition was changed significantly for M1-40TiO₂-SM, in which the Te was associated with C–H cleavage and active oxygen species was enriched on the surface [66–68]. It also can be seen that no change was detected on the surface compositions and valence states in Mo, Nb, Te, and Ti elements in the 24 h time-on-stream tests.

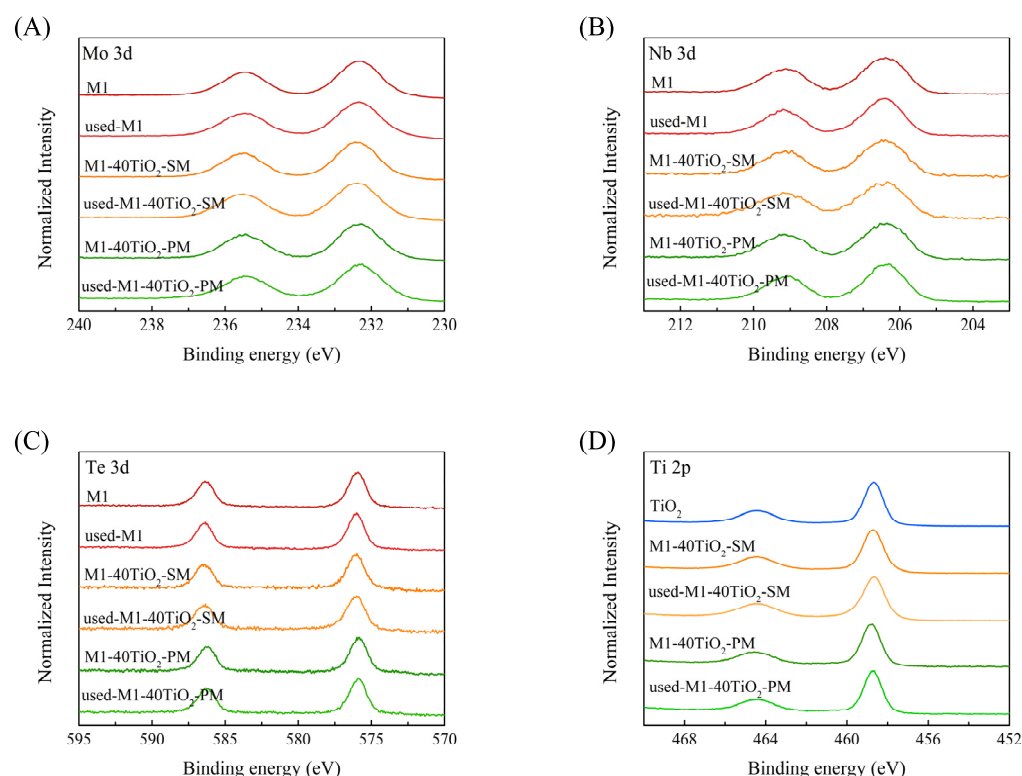


Figure 8. XPS spectra of the fresh and used catalysts (M1, M1-40TiO₂-SM, M1-40TiO₂-PM, and TiO₂): (A) Mo 3d; (B) Nb 3d; (C) Te 3d; and (D) Ti 2p.

Figure 9 illustrates the XPS spectra of vanadium on the fresh and used samples (M1, M1-40TiO₂-SM, and M1-40TiO₂-PM). The V 2p_{3/2} peak could be fitted into two phases at 516.3 ± 0.1 eV and 517.1 ± 0.1 eV, corresponding to the V⁴⁺ and V⁵⁺ species, respectively [69,70]. As shown in Table 4, the V⁵⁺/V⁴⁺ ratios of catalysts M1-40TiO₂-SM and M1-40TiO₂-PM increased considerably due to the introduction of TiO₂, which is the important reason for promoting remarkably the catalytic performance. The ratio of the vanadium valence states of the M1-40TiO₂-SM catalyst (V⁵⁺/V⁴⁺ ratio = 1.18) was higher than that of the M1-40TiO₂-PM catalyst (V⁵⁺/V⁴⁺ ratio = 1.10), which was consistent with the result of the evaluation in Section 3.1.1. Moreover, the decrease of the catalytic performance of the used M1-40TiO₂-SM catalyst (in Section 3.1.2) was accompanied by the decrease of the V⁵⁺/V⁴⁺ ratio, which has also been proved that the amount of V⁵⁺ in catalysts significantly influenced the catalytic activity in the ODHE reaction, just as reported in the reference [32]. Unlike the M1-40TiO₂-SM catalyst, the used M1-40TiO₂-PM catalyst showed a slight promotion in the 24 h time-on-stream test, which may be caused by the synergistic effect of the decrease of the V⁵⁺/V⁴⁺ ratio and the increase of the specific surface area of the used M1-40TiO₂-PM catalyst.

3.2.5. H₂-TPR and C₂H₆-TPSR Characterizations

It is widely accepted that the ODHE process catalyzed by M1 catalyst follows the MvK mechanism, in which the lattice oxygen species is responsible for the cleavage of the C–H bond in ethane [71,72]. Therefore, there must be some correlation between the activity of lattice oxygen species and the catalytic performance of the catalyst. Hence, we conducted the H₂-TPR and C₂H₆-TPSR characterizations to evaluate the amount and activity of oxygen species, which may contribute to the catalytic activity. As shown in Figure 10, broad peaks in the range of 300–650 °C were observed for all samples, except for TiO₂. After introducing the TiO₂, the peak position was shifts from 550 to 520 °C and 504 °C for M1-40TiO₂-PM and M1-40TiO₂-SM, respectively. In addition, for the M1-40TiO₂-SM sample, an additional peak was observed at about 420 °C. The new peak might correlate

with surface oxygen species (electrophilic oxygen species) and had a negative effect for the ethylene selectivity [73,74], as shown in Section 3.1.1. Moreover, the H₂ consumption decreased after the introduction of the TiO₂ phase, which implied the decreased amount of available lattice oxygen species.

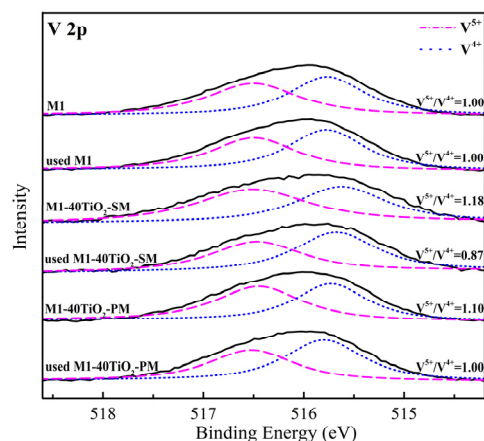


Figure 9. XPS spectra of V 2p_{3/2} for the fresh and used catalysts (M1, M1-40TiO₂-SM, and M1-40TiO₂-PM).

Table 4. Ratios of the vanadium valence states and the surface compositions of the fresh and used catalysts in the ODHE process.

Catalyst	V ⁵⁺ /V ⁴⁺ Ratio	Surface Composition
M1	1.00	MoV _{0.10} Nb _{0.34} Te _{0.21}
Used M1	1.00	MoV _{0.10} Nb _{0.34} Te _{0.21}
M1-40TiO ₂ -SM	1.18	MoV _{0.11} Nb _{0.33} Te _{0.34}
Used M1-40TiO ₂ -SM	0.87	MoV _{0.11} Nb _{0.32} Te _{0.32}
M1-40TiO ₂ -PM	1.10	MoV _{0.11} Nb _{0.36} Te _{0.21}
Used M1-40TiO ₂ -PM	1.10	MoV _{0.11} Nb _{0.36} Te _{0.21}

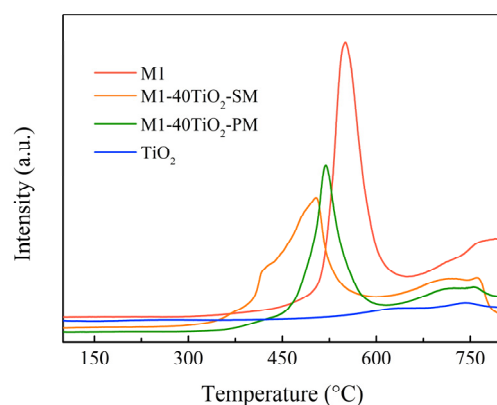


Figure 10. H₂ temperature-programmed reduction (H₂-TPR) results of different catalysts (M1, M1-40TiO₂-SM, M1-40TiO₂-PM, and TiO₂).

Figure 11A–F shows the C₂H₆-TPSR profiles for all samples. As shown in Figure 11A, peaks at about ~400, ~580, and ~640 °C can be observed for C₂H₄ signals. It should be noted that the reaction temperature of ODHE based on the M1 catalyst was in the range of 300 to 500 °C and the peak at about ~400 °C was more relevant. After the introduction of TiO₂, the peak position shifted from 420 to 405 and 395 °C for M1-40TiO₂-PM and M1-40TiO₂-SM, respectively.

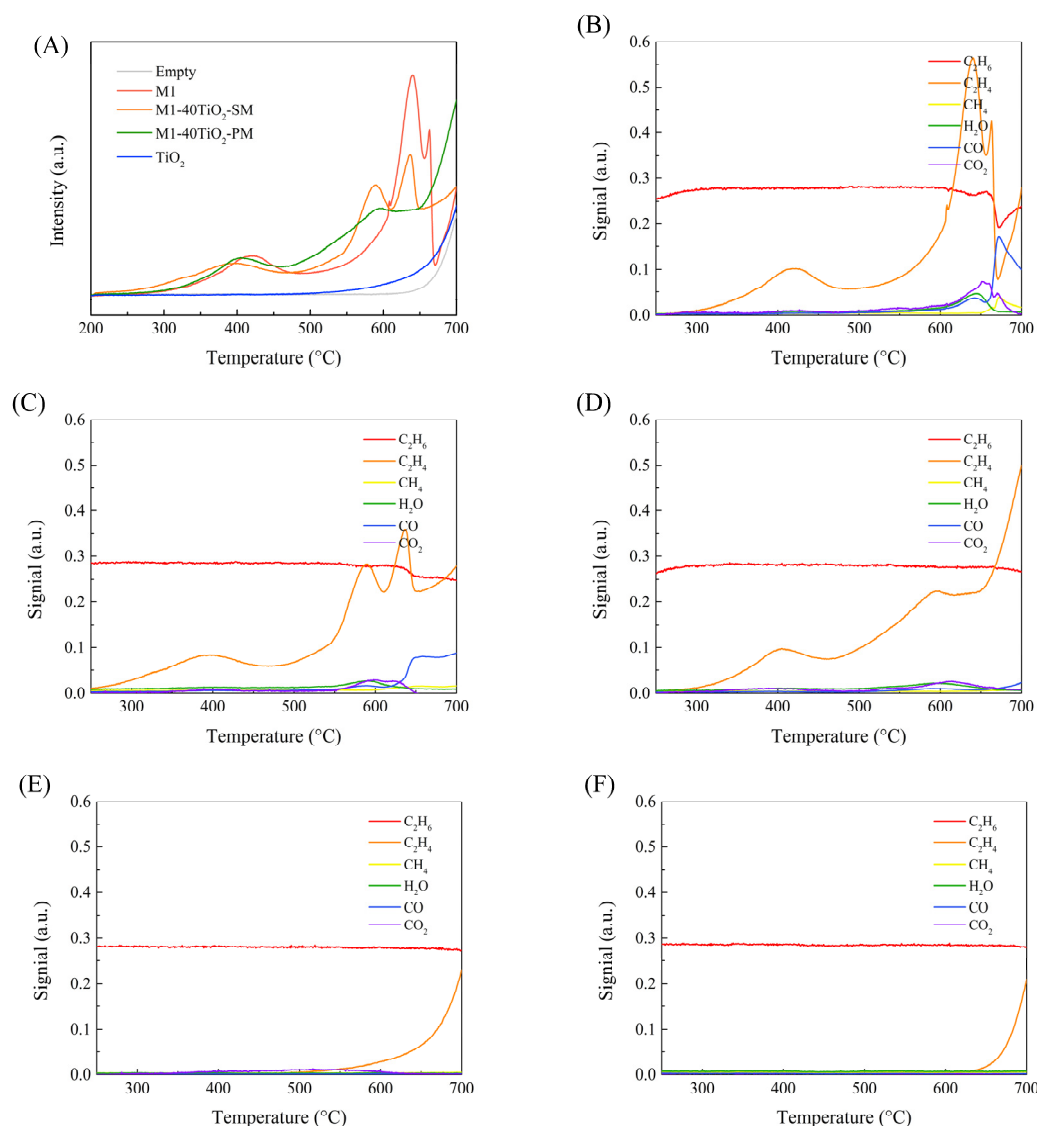


Figure 11. (A) C₂H₄ signals of the C₂H₆-TPSR profiles for different catalysts. C₂H₆-TPSR profiles of different catalysts: (B) M1; (C) M1-40TiO₂-SM; (D) M1-40TiO₂-PM; (E) TiO₂; and (F) empty tube.

In addition, the peaks area at ~400 °C had a positive correlation with the catalyst activity (M1-40TiO₂-SM > M1-40TiO₂-PM > M1), which indicated a difference in the amount of active oxygen species available for the C–H bond cleavage in different catalysts. Besides, at high reduction temperatures, there were huge differences among different catalysts (which may be related to thermal cracking reaction or coke formation). In conclusion, both H₂-TPR and C₂H₆-TPSR profiles demonstrated that the introduction of TiO₂ by the physical mixing method or sol-gel method significantly affected the reduction properties and the amount of available oxygen species for the cleavage of C–H bonds, which may contribute to the activity of M1 catalysts for the ODHE process. Moreover, the differences of the H₂-TPR and C₂H₆-TPSR profiles between M1-40TiO₂-SM and M1-40TiO₂-PM implied the presence of different promotion mechanisms underlying the M1–TiO₂ nanocomposite, which may be caused by the different interaction mechanisms between TiO₂ and M1 prepared by different methods.

3.2.6. Raman Spectra

Figure 12 shows the Raman spectra of M1 and M1-40TiO₂-PM/SM samples including the reference material (TiO₂). The peaks corresponding to M1 (872 and 792 cm⁻¹) [60]

and anatase-phase TiO_2 (148 , 400 , 522 , and 643 cm^{-1}) [75] were detected. The M1-40 TiO_2 -PM/SM samples showed different relative intensities about the M1 and anatase-phase TiO_2 in Raman spectra, and the relative intensity of TiO_2 in M1-40 TiO_2 -SM was increased. The results are consistent with Figures 6 and 7, in which the TiO_2 particles were well dispersed in SM samples. There was no other peak detected, which implied that no change took place in the M1 and TiO_2 during the preparation procedure.

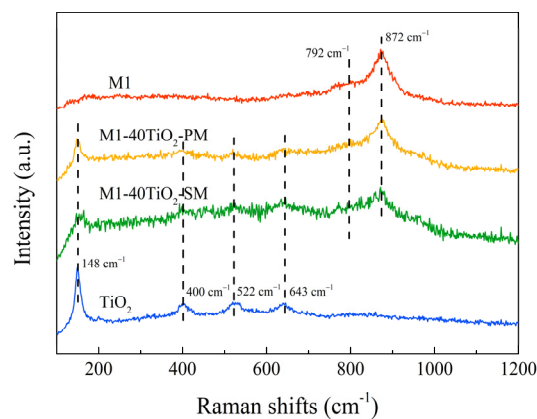


Figure 12. Raman spectra of different catalysts.

4. Conclusions

Catalysts of 40 wt.% TiO_2 introduced to a phase-pure M1 were prepared by the sol-gel method and the physical mixing method and evaluated in a fixed bed reactor for the ODHE process. Many characterization methods were applied to reveal the effects of TiO_2 introduced by different methods. It was found that the introduction of TiO_2 to the phase-pure M1 by two methods can both effectively promote the catalytic performance. Compared to the M1-40 TiO_2 -PM catalyst, the M1-40 TiO_2 -SM catalyst presented a higher STY of ethylene of 0.67 $\text{kg}_{\text{C}_2\text{H}_4}/\text{kg}_{\text{cat}}/\text{h}$, showing an increase by 76% than that of the phase-pure M1 catalyst at the reaction temperature of 400 $^\circ\text{C}$. The introduction of TiO_2 to the phase-pure M1 can significantly increase the activity of oxygen species and improve the oxidative state of vanadium species on the surface of catalysts M1-40 TiO_2 -SM and M1-40 TiO_2 -PM, which was proved as an essential factor in enhancing the catalytic performance in the ODHE reaction. However, in comparison with the physical mixing method, the sol-gel method changed the surface composition of the M1 phase significantly. H_2 -TPR and C_2H_6 -TPSR profiles also demonstrated the difference of oxygen species between M1-40 TiO_2 -SM and M1-40 TiO_2 -PM. Moreover, the structure design of the M1- TiO_2 -SM nanocomposite (e.g., a wrapped structure [76]) will be interesting for the improvement of the catalytic performance. Though the sol-gel method beneficial for generating a better catalytic performance, the M1-40 TiO_2 -PM can reach a higher catalytic efficiency at a high operation temperature and showed a superior stability in the long-term test. More details deserve further investigation to improve the catalytic activity of the M1-40 TiO_2 -PM catalyst, as the physical mixing method is simpler than the sol-gel method.

Author Contributions: Conceptualization, Y.C. (Yuxin Chen) and D.D.; methodology, Y.C. (Yuxin Chen) and D.D.; validation, Y.C. (Yuxin Chen) and D.D.; formal analysis, Y.C. (Yuxin Chen), D.D. and B.Y.; investigation, Y.C. (Yuxin Chen) and D.D.; resources, B.Y. and Y.C. (Yi Cheng); data curation, Y.C. (Yuxin Chen) and D.D.; writing—original draft preparation Y.C. (Yuxin Chen); writing—review and editing, Y.C. (Yuxin Chen), D.D., B.Y. and Y.C. (Yi Cheng); visualization, Y.C. (Yuxin Chen) and D.D.; supervision, Y.C. (Yi Cheng); funding acquisition, Y.C. (Yi Cheng). All authors have read and agreed to the published version of the manuscript.

Funding: This research was funded by the National Natural Science Foundation of China (No. 21776156).

Data Availability Statement: Not available.

Acknowledgments: The authors would like to acknowledge the financial support from the National Natural Science Foundation of China (No. 21776156).

Conflicts of Interest: The authors declare that they have no known competing financial interests or personal relationships that could have appeared to influence the work reported in this paper.

References

1. Gartner, C.A.; van Veen, A.C.; Lercher, J.A. Oxidative Dehydrogenation of Ethane: Common Principles and Mechanistic Aspects. *ChemCatChem* **2013**, *5*, 3196–3217. [[CrossRef](#)]
2. Najari, S.; Saeidi, S.; Concepcion, P.; Dionysiou, D.D.; Bhargava, S.K.; Lee, A.F.; Wilson, K. Oxidative dehydrogenation of ethane: Catalytic and mechanistic aspects and future trends. *Chem. Soc. Rev.* **2021**, *50*, 4564–4605. [[CrossRef](#)]
3. Zhu, H.D.C.; Rosenfeld, M.; Harb, D.H.; Anjum, M.N.; Hedhili, S.; Ould-Chikh, J.-M. Basset. Ni–M–O (M = Sn, Ti, W) Catalysts Prepared by a Dry Mixing Method for Oxidative Dehydrogenation of Ethane. *ACS Catal.* **2016**, *6*, 2852–2866. [[CrossRef](#)]
4. Solsona, B.; Ivars, F.; Dejoz, A.; Concepcion, P.; Vázquez, M.I.; Nieto, J.M.L. Supported Ni–W–O Mixed Oxides as Selective Catalysts for the Oxidative Dehydrogenation of Ethane. *Top. Catal.* **2009**, *52*, 751–757. [[CrossRef](#)]
5. Botella, P.; Garcia-Gonzalez, E.; Dejoz, A.; Nieto, J.M.L.; Vazquez, M.I.; Gonzalez-Calbet, J. Selective Oxidative Dehydrogenation of Ethane on MoVTeNbO Mixed Metal Oxide Catalysts. *J. Catal.* **2004**, *225*, 428–438. [[CrossRef](#)]
6. Nieto, L.; José, M. The Selective Oxidative Activation of Light Alkanes. From Supported Vanadia to Multicomponent Bulk V-Containing Catalysts. *Top. Catal.* **2006**, *41*, 3–15. [[CrossRef](#)]
7. Botella, P.; Dejoz, A.; Nieto, J.L.; Concepción, P.; Vázquez, M. Selective oxidative dehydrogenation of ethane over MoVSbO mixed oxide catalysts. *Appl. Catal. A Gen.* **2006**, *298*, 16–23. [[CrossRef](#)]
8. Heracleous, E.; Lemonidou, A. Ni–Nb–O mixed oxides as highly active and selective catalysts for ethene production via ethane oxidative dehydrogenation. Part II: Mechanistic aspects and kinetic modeling. *J. Catal.* **2006**, *237*, 175–189. [[CrossRef](#)]
9. Chu, B.; An, H.; Nijhuis, T.; Schouten, J.C.; Cheng, Y. A self-redox pure-phase M1 MoVNbTeO/CeO₂ nanocomposite as a highly active catalyst for oxidative dehydrogenation of ethane. *J. Catal.* **2015**, *329*, 471–478. [[CrossRef](#)]
10. Nguyen, T.T.; Aouine, M.; Millet, J.M.M. Optimizing the Efficiency of MoVNbTeO Catalysts for Ethane Oxidative Dehydrogenation to Ethylene. *Catal. Commun.* **2012**, *21*, 22–26. [[CrossRef](#)]
11. Nieto, J.M.L.; Solsona, B.; Grasselli, R.K.; Concepción, P. Promoted NiO Catalysts for the Oxidative Dehydrogenation of Ethane. *Top. Catal.* **2014**, *57*, 1248–1255. [[CrossRef](#)]
12. Popescu, I.; Heracleous, E.; Skoufa, Z.; Lemonidou, A.; Marcu, I.-C. Study by electrical conductivity measurements of semiconductive and redox properties of M-doped NiO (M = Li, Mg, Al, Ga, Ti, Nb) catalysts for the oxidative dehydrogenation of ethane. *Phys. Chem. Chem. Phys.* **2014**, *16*, 4962–4970. [[CrossRef](#)] [[PubMed](#)]
13. Xin, C.; Wang, F.; Xu, G.Q. Tuning surface V⁵⁺ concentration in M1 phase MoVSbO_x catalysts for ethylene production from ethane through oxidative dehydrogenation reaction. *Appl. Catal. A Gen.* **2021**, *610*, 117946. [[CrossRef](#)]
14. Gao, Y.; Neal, L.M.; Li, F. Li-Promoted La_xSr_{2-x}FeO_{4-δ} Core-Shell Redox Catalysts for Oxidative Dehydrogenation of Ethane under a Cyclic Redox Scheme. *ACS Catal.* **2016**, *6*, 7293–7302. [[CrossRef](#)]
15. Baca, M.; Millet, J.M.M. Bulk Oxidation State of the Different Cationic Elements in the MoVTe(Sb)NbO Catalysts for Oxidation or Ammoxidation of Propane. *Appl. Catal. A Gen.* **2005**, *279*, 67–77. [[CrossRef](#)]
16. Ishikawa, S.; Yi, X.; Murayama, T.; Ueda, W. Heptagonal channel micropore of orthorhombic Mo₃VO_x as catalysis field for the selective oxidation of ethane. *Appl. Catal. A Gen.* **2014**, *474*, 10–17. [[CrossRef](#)]
17. Zhang, Z.Q.; Ding, J.; Chai, R.J.; Zhao, G.F.; Liu, Y.; Lu, Y. Oxidative Dehydrogenation of Ethane to Ethylene: A Promising CeO₂-ZrO₂-Modified NiO-Al₂O₃/Ni-Foam Catalyst. *Appl. Catal. A Gen.* **2018**, *550*, 151–159. [[CrossRef](#)]
18. Bortolozzi, J.; Banús, E.; Terzaghi, D.; Gutierrez, L.; Milt, V.; Ulla, M. Novel catalytic ceramic papers applied to oxidative dehydrogenation of ethane. *Catal. Today* **2013**, *216*, 24–29. [[CrossRef](#)]
19. Melzer, D.; Mestl, G.; Wanninger, K.; Zhu, Y.; Browning, N.D.; Sanchez-Sanchez, M.; Lercher, J.A. Design and Synthesis of Highly Active MoVTeNb-Oxides for Ethane Oxidative Dehydrogenation. *Nat. Commun.* **2019**, *10*, 4012. [[CrossRef](#)] [[PubMed](#)]
20. Ding, W.; Zhao, K.; Jiang, S.; Zhao, Z.; Cao, Y.; He, F. Alkali-metal enhanced LaMnO₃ perovskite oxides for chemical looping oxidative dehydrogenation of ethane. *Appl. Catal. A Gen.* **2021**, *609*, 117910. [[CrossRef](#)]
21. Zhu, H.; Ould-Chikh, S.; Anjum, D.H.; Sun, M.; Biaisque, G.; Basset, J.M.; Caps, V. Nb effect in the nickel oxide-catalyzed low-temperature oxidative dehydrogenation of ethane. *J. Catal.* **2012**, *285*, 292–303. [[CrossRef](#)]
22. Delgado, D.; Sanchis, R.; Cecilia, J.A.; Rodriguez-Castellon, E.; Caballero, A.; Solsona, B.; Nieto, J.M.L. Support Effects on NiO-Based Catalysts for the Oxidative Dehydrogenation (ODH) of Ethane. *Catal. Today* **2019**, *333*, 10–16. [[CrossRef](#)]
23. Wang, C.; Yang, B.; Gu, Q.; Han, Y.; Tian, M.; Su, Y.; Pan, X.; Kang, Y.; Huang, C.; Liu, H.; et al. Near 100% ethene selectivity achieved by tailoring dual active sites to isolate dehydrogenation and oxidation. *Nat. Commun.* **2021**, *12*, 5447. [[CrossRef](#)]
24. Ishchenko, E.; Kardash, T.; Gulyaev, R.; Sobolev, V.; Bondareva, V. Effect of K and Bi doping on the M1 phase in MoVTeNbO catalysts for ethane oxidative conversion to ethylene. *Appl. Catal. A Gen.* **2016**, *514*, 1–13. [[CrossRef](#)]
25. Watanabe, H.; Koyasu, Y. New Synthesis Route for Mo–V–Nb–Te Mixed Oxides Catalyst for Propane Ammoxidation. *Appl. Catal. A Gen.* **2000**, *194–195*, 479–485. [[CrossRef](#)]

26. Xie, Q.; Chen, L.; Weng, W.; Wan, H. Preparation of MoVTe(Sb)Nb Mixed Oxide Catalysts Using a Slurry Method for Selective Oxidative Dehydrogenation of Ethane. *J. Mol. Catal. A Chem.* **2005**, *240*, 191–196. [[CrossRef](#)]
27. Grasselli, R.K. Selectivity issues in (amm)oxidation catalysis. *Catal. Today* **2005**, *99*, 23–31. [[CrossRef](#)]
28. Deniau, B.; Bergeret, G.; Jouguet, B.; Dubois, J.L.; Millet, J.M.M. Preparation of Single M1 Phase MoVTe(Sb)NbO Catalyst: Study of the Effect of M2 Phase Dissolution on the Structure and Catalytic Properties. *Top. Catal.* **2008**, *50*, 33–42. [[CrossRef](#)]
29. Nieto, J.L.; Solsona, B.; Concepción, P.; Ivars, F.; Dejoz, A.; Vázquez, M. Reaction products and pathways in the selective oxidation of C2–C4 alkanes on MoVTeNb mixed oxide catalysts. *Catal. Today* **2010**, *157*, 291–296. [[CrossRef](#)]
30. Li, X.; Douglas, J.; Douglas, B.; Blom, A.; Vogt, T. Improvement of the Structural Model for the M1 Phase Mo–V–Nb–Te–O Propane (Amm)Oxidation Catalyst. *Top. Catal.* **2011**, *54*, 614–626. [[CrossRef](#)]
31. Deniau, B.; Nguyen, T.T.; Delichere, P.; Safonova, O.; Millet, J.M.M. Redox State Dynamics at the Surface of MoVTe(Sb)NbO M1 Phase in Selective Oxidation of Light Alkanes. *Top. Catal.* **2013**, *56*, 1952–1962. [[CrossRef](#)]
32. Grasselli, R.K.; Douglas, J.B.; Peter, D., Jr.; James, D.B.; Claus, G.L.; Anthony, F.V.; Weingand, T. Active Centers in Mo–V–Nb–Te–O (amm)Oxidation Catalysts. *Catal. Today* **2004**, *91–92*, 251–258. [[CrossRef](#)]
33. Nguyen, T.; Burel, L.; Nguyen, D.; Pham-Huu, C.; Millet, J. Catalytic performance of MoVTeNbO catalyst supported on SiC foam in oxidative dehydrogenation of ethane and ammoxidation of propane. *Appl. Catal. A Gen.* **2012**, *433–434*, 41–48. [[CrossRef](#)]
34. Havecker, M.; Wrabetz, S.; Krohnert, J.; Csepei, L.L.; d’Alnoncourt, R.N.; Kolen’ko, Y.V.; Girgsdies, F.; Schlogl, R.; Trunschke, A. Surface Chemistry of Phase-Pure M1 MoVTeNbO Oxide During Operation in Selective Oxidation of Propane to Acrylic Acid. *J. Catal.* **2012**, *285*, 48–60. [[CrossRef](#)]
35. Sanfilippo, D.; Miracca, I. Dehydrogenation of paraffins: Synergies between catalyst design and reactor engineering. *Catal. Today* **2006**, *111*, 133–139. [[CrossRef](#)]
36. Cavani, F.; Ballarini, N.; Cericola, A. Oxidative Dehydrogenation of Ethane and Propane: How Far from Commercial Implementation? *Catal. Today* **2007**, *127*, 113–131. [[CrossRef](#)]
37. Schmidt, L.D.; Siddall, J.; Bearden, M. New ways to make old chemicals. *AIChE J.* **2000**, *46*, 1492–1495. [[CrossRef](#)]
38. Wang, H.; Gu, X.-K.; Zheng, X.; Pan, H.; Zhu, J.; Chen, S.; Cao, L.; Li, W.-X.; Lu, J. Disentangling the size-dependent geometric and electronic effects of palladium nanocatalysts beyond selectivity. *Sci. Adv.* **2019**, *5*, eaat6413. [[CrossRef](#)] [[PubMed](#)]
39. Mishanin, I.I.; Bogdan, V.I. Regularities of Oxidative Dehydrogenation of Ethane Over MoVNbTeOx Catalyst Under Supercritical Conditions. *Catal. Lett.* **2020**, *151*, 2088–2093. [[CrossRef](#)]
40. Mishanin, I.I.; Viktor, I.B. Advantages of Ethane Oxidative Dehydrogenation on the MoVNbTeOx Catalyst under Elevated Pressure. *Mendeleev Commun.* **2019**, *29*, 455–457. [[CrossRef](#)]
41. Chu, B.; Truter, L.; Nijhuis, T.A.; Cheng, Y. Oxidative dehydrogenation of ethane to ethylene over phase-pure M1 MoVNbTeOx catalysts in a micro-channel reactor. *Catal. Sci. Technol.* **2015**, *5*, 2807–2813. [[CrossRef](#)]
42. Chen, J.K.; Bollini, P.; Balakotaiah, V. Oxidative Dehydrogenation of Ethane over Mixed Metal Oxide Catalysts: Autothermal or Cooled Tubular Reactor Design? *AIChE J.* **2021**, *67*, e17168. [[CrossRef](#)]
43. Galina, A.Z.; Shutilov, A.A.; Bondareva, V.M.; Sobolev, V.I.; Marchuk, A.S.; Tsybulya, S.V.; Prosvirin, I.P.; Ishchenko, A.V.; Gavrilov, V.Y. New Multicomponent MoVSbNbCeOx/SiO₂ Catalyst with Enhanced Catalytic Activity for Oxidative Dehydrogenation of Ethane to Ethylene. *ChemCatChem* **2020**, *12*, 4149–4159.
44. Yun, Y.S.; Lee, M.; Sung, J.; Yun, D.; Kim, T.Y.; Park, H.; Lee, K.R.; Song, C.K.; Kim, Y.; Lee, J.; et al. Promoting Effect of Cerium on MoVTeNbO Mixed Oxide Catalyst for Oxidative Dehydrogenation of Ethane to Ethylene. *Appl. Catal. B Environ.* **2018**, *237*, 554–562. [[CrossRef](#)]
45. Dang, D.; Chen, X.; Yan, B.H.; Li, Y.K.; Cheng, Y. Catalytic Performance of Phase-Pure M1 MoVTeNbOx/CeO₂ Composite for Oxidative Dehydrogenation of Ethane. *J. Catal.* **2018**, *365*, 238–248. [[CrossRef](#)]
46. de Arriba, A.; Solsona, B.; Dejoz, A.M.; Concepción, P.; Homs, N.; de la Piscina, P.R.; Nieto, J.M.L. Evolution of the optimal catalytic systems for the oxidative dehydrogenation of ethane: The role of adsorption in the catalytic performance. *J. Catal.* **2021**. [[CrossRef](#)]
47. Annamalai, L.; Ezenwa, S.; Dang, Y.; Tan, H.; Suib, S.L.; Deshlahra, P. Comparison of structural and catalytic properties of monometallic Mo and V oxides and M1 phase mixed oxides for oxidative dehydrogenation. *Catal. Today* **2020**, *368*, 28–45. [[CrossRef](#)]
48. Donaubaue, P.J.; Melzer, D.M.; Wanninger, K.; Mestl, G.; Sanchez-Sanchez, M.; Lercher, J.A.; Hinrichsen, O. Intrinsic kinetic model for oxidative dehydrogenation of ethane over MoVTeNb mixed metal oxides: A mechanistic approach. *Chem. Eng. J.* **2019**, *383*, 123195. [[CrossRef](#)]
49. Chen, X.; Dang, D.; An, H.; Chu, B.; Cheng, Y. MnO Promoted Phase-Pure M1 MoVTeNb Oxide for Ethane Oxidative Dehydrogenation. *J. Taiwan Inst. Chem. Eng.* **2019**, *95*, 103–111. [[CrossRef](#)]
50. Wijaya, K.; Putri, A.R.; Sudiono, S.; Mulijani, S.; Patah, A.; Wibowo, A.C.; Saputri, W.D. Effectively Synthesizing SO₄/TiO₂ Catalyst and Its Performance for Converting Ethanol into Diethyl Ether (DEE). *Catalysts* **2021**, *11*, 1492. [[CrossRef](#)]
51. Serga, V.; Burve, R.; Krumina, A.; Romanova, M.; Kotomin, E.; Popov, A. Extraction–Pyrolytic Method for TiO₂ Polymorphs Production. *Crystals* **2021**, *11*, 431. [[CrossRef](#)]
52. Chung, Y.-C.; Xie, P.-J.; Lai, Y.-W.; Lo, A.-Y. Hollow TiO₂ Microsphere/Graphene Composite Photocatalyst for CO₂ Photoreduction. *Catalysts* **2021**, *11*, 1532. [[CrossRef](#)]

53. Holmberg, J.; Haggblad, R.; Andersson, A. A Study of Propane Ammoxidation on Mo–V–Nb–Te-Oxide Catalysts Diluted with Al₂O₃, SiO₂, and TiO₂. *J. Catal.* **2006**, *243*, 350–359. [[CrossRef](#)]
54. Li, X.; Iglesia, E. Support and promoter effects in the selective oxidation of ethane to acetic acid catalyzed by Mo-V-Nb oxides. *Appl. Catal. A Gen.* **2008**, *334*, 339–347. [[CrossRef](#)]
55. Che-Galicia, G.; Ruiz-Martínez, R.S.; López-Isunza, F.; Castillo-Araiza, C.O. Modeling of Oxidative Dehydrogenation of Ethane to Ethylene on a MoVNbTeO/TiO₂ Catalyst in an Industrial-Scale Packed Bed Catalytic Reactor. *Chem. Eng. J.* **2015**, *280*, 682–694. [[CrossRef](#)]
56. Dang, D.; Chen, Y.; Chen, X.; Feng, K.; Yan, B.; Cheng, Y. Phase-pure M1 MoVNbTeOx/TiO₂ nanocomposite catalysts: Highly catalytic performance for oxidative dehydrogenation of ethane. *Catal. Sci. Technol.* **2022**. [[CrossRef](#)]
57. Chu, B.; Truter, L.; Nijhuis, T.A.; Cheng, Y. Performance of Phase-Pure M1 MoVNbTeOx Catalysts by Hydrothermal Synthesis with Different Post-Treatments for the Oxidative Dehydrogenation of Ethane. *Appl. Catal. A Gen.* **2015**, *498*, 99–106. [[CrossRef](#)]
58. Chen, X.; Yang, Q.; Chu, B.; An, H.; Cheng, Y. Valence Variation of Phase-Pure M1 MoVNbTeOx Oxide by Plasma Treatment for Improved Catalytic Performance in Oxidative Dehydrogenation of Ethane. *RSC Adv.* **2015**, *5*, 91295–91301. [[CrossRef](#)]
59. Perez-Ramirez, J.; Berger, R.J.; Mul, G.; Kapteijn, F.; Moulijn, J.A. The Six-Flow Reactor Technology—A Review on Fast Catalyst Screening and Kinetic Studies. *Catal. Today* **2000**, *60*, 93–109. [[CrossRef](#)]
60. Solsona, B.; Vazquez, M.; Ivars, F.; Dejoz, A.; Concepcion, P.; Lopeznieto, J. Selective Oxidation of Propane and Ethane on Diluted Mo–V–Nb–Te Mixed-Oxide Catalysts. *J. Catal.* **2007**, *252*, 271–280. [[CrossRef](#)]
61. Huerta, M.V.M.; Gao, X.; Tian, H.; Wachs, I.; Fierro, J.; Bñares, M. Oxidative dehydrogenation of ethane to ethylene over alumina-supported vanadium oxide catalysts: Relationship between molecular structures and chemical reactivity. *Catal. Today* **2006**, *118*, 279–287.
62. Grant, J.T.; Venegas, J.M.; McDermott, W.; Hermans, I. Aerobic Oxidations of Light Alkanes over Solid Metal Oxide Catalysts. *Chem. Rev.* **2017**, *118*, 2769–2815. [[CrossRef](#)]
63. Andrushkevich, T.V.; Popova, G.Y.; Chesalov, Y.A.; Ischenko, E.V.; Khramov, M.I.; Kaichev, V.V. Propane Ammoxidation on Bi Promoted MoVTeNbOx Oxide Catalysts: Effect of Reaction Mixture Composition. *Appl. Catal. A Gen.* **2015**, *506*, 109–117. [[CrossRef](#)]
64. Botella, P.; García-González, E.; Nieto, J.M.L.; Gonzalez-Calbet, J.M. MoVTeNbO multifunctional catalysts: Correlation between constituent crystalline phases and catalytic performance. *Solid State Sci.* **2005**, *7*, 507–519. [[CrossRef](#)]
65. Tao, F.; Shen, Y.; Liang, Y.; Li, H. Synthesis and Characterization of Co(OH)₂/TiO₂ Nanotube Composites as Supercapacitor Materials. *J. Solid State Electrochem.* **2006**, *11*, 853–858. [[CrossRef](#)]
66. Cheng, M.J.; Goddard, W.A., 3rd. In Silico Design of Highly Selective Mo-V-Te-Nb-O Mixed Metal Oxide Catalysts for Ammoxidation and Oxidative Dehydrogenation of Propane and Ethane. *J. Am. Chem. Soc.* **2015**, *137*, 13224–13227. [[CrossRef](#)] [[PubMed](#)]
67. Valente, J.S.; Armendáriz-Herrera, H.; Solorzano, R.Q.; Del Ángel, P.; Nava, N.; Massó, A.; Nieto, J.M.L. Chemical, Structural, and Morphological Changes of a MoVTeNb Catalyst during Oxidative Dehydrogenation of Ethane. *ACS Catal.* **2014**, *4*, 1292–1301. [[CrossRef](#)]
68. Aouine, M.; Epicier, T.; Millet, J.-M.M. In Situ Environmental STEM Study of the MoVTe Oxide M1 Phase Catalysts for Ethane Oxidative Dehydrogenation. *ACS Catal.* **2016**, *6*, 4775–4781. [[CrossRef](#)]
69. Guan, J.; Wu, S.; Wang, H.; Jing, S.; Wang, G.; Zhen, K.; Kan, Q. Synthesis and characterization of MoVTeCeO catalysts and their catalytic performance for selective oxidation of isobutane and isobutylene. *J. Catal.* **2007**, *251*, 354–362. [[CrossRef](#)]
70. Demeter, M.; Neumann, M.; Reichelt, W. Mixed-valence vanadium oxides studied by XPS. *Surf. Sci.* **2000**, *454–456*, 41–44. [[CrossRef](#)]
71. Botella, P.; Dejoz, A.; Abello, M.C.; Vázquez, M.I.; Arrúa, L.; Nieto, J.M.L. Selective Oxidation of Ethane: Developing an Orthorhombic Phase in Mo–V–X (X=Nb, Sb, Te) Mixed Oxides. *Catal. Today* **2009**, *142*, 272–277. [[CrossRef](#)]
72. Zhao, X.; Zhang, C.; Xu, C.; Li, H.; Huang, H.; Song, L.; Li, X. Kinetics study for the oxidative dehydrogenation of ethyl lactate to ethyl pyruvate over MoVNbO based catalysts. *Chem. Eng. J.* **2016**, *296*, 217–224. [[CrossRef](#)]
73. Liu, J.; Mohamed, F.; Sauer, J. Selective oxidation of propene by vanadium oxide monomers supported on silica. *J. Catal.* **2014**, *317*, 75–82. [[CrossRef](#)]
74. Kwon, S.; Deshlahra, P.; Iglesia, E. Dioxygen activation routes in Mars-van Krevelen redox cycles catalyzed by metal oxides. *J. Catal.* **2018**, *364*, 228–247. [[CrossRef](#)]
75. Zhu, J.; Ren, J.; Huo, Y.N.; Bian, Z.F.; Li, H.X. Nanocrystalline Fe/TiO₂ Visible Photocatalyst with a Mesoporous Structure Prepared Via a Nonhydrolytic Sol-Gel Route. *J. Phys. Chem. C* **2007**, *111*, 18965–18969. [[CrossRef](#)]
76. Feng, K.; Wang, S.; Zhang, D.; Wang, L.; Yu, Y.; Feng, K.; Li, Z.; Zhu, Z.; Li, C.; Cai, M.; et al. Cobalt Plasmonic Superstructures Enable Almost 100% Broadband Photon Efficient CO₂ Photocatalysis. *Adv. Mater.* **2020**, *32*, 2000014. [[CrossRef](#)]